

Unveiling the Role of Magnetic Field in Generating Quasi-Periodic Oscillations: Insights from Accreting White Dwarf Systems

M. Veresvarska^{a,b,c,*} and S. Scaringi^{a,d}

^a*Department of Physics, Centre for Extragalactic Astronomy, Durham University, South Road, Durham DH1 3LE, UK,*

^b*Institute of Space Sciences (ICE, CSIC), Campus UAB, Carrer de Can Magrans s/n, Barcelona, E-08193, Spain*

^c*Institut d'Estudis Espacials de Catalunya (IEEC), Barcelona, E-08034, Spain*

^d*INAF – Osservatorio Astronomico di Capodimonte, Salita Moiariello 16, I-80131 Naples, Italy*

E-mail: mveresvarska@ice.csic.es

Magnetic fields, whether originating from the compact object or the accretion disc, play an important but often neglected role in shaping the geometry and variability of accretion flows. Recently quasi-periodic variability in accreting white dwarfs has pointed towards a mechanism of driving the precession of the inner accretion flow through misaligned accretor magnetic field. This is presenting an alternative explanation for the well known quasi-periodic oscillations (QPOs) in X-ray binaries and has shown promise in application to QPOs in pulsating ultraluminous X-ray sources with extremely high magnetic fields. However, further detections of these QPOs in accreting white dwarfs are needed to test their behaviour and adherence to the model. However, the prevalence and properties of such QPOs in accreting white dwarfs remain poorly constrained due to the limited number of detections. Here, we report the detection of a new QPO in the WZ Sge type dwarf nova BW Scl and present a comprehensive reanalysis of previously detected accreting white dwarf (AWD) QPOs without reliance on fiducial parameter assumptions. These results demonstrate that QPOs can be used to place constraints on magnetic field strengths and other system properties of nominally non-magnetic white dwarfs.

87th Fujihara Seminar: The 50th Anniversary Workshop of the Disk Instability Model in Compact Binary Stars

Tomakomai, Japan

22-26 September 2025

*Speaker

© Copyright owned by the author(s) under the terms of the Creative Commons Attribution-NonCommercial-NoDerivatives 4.0 International License (CC BY-NC-ND 4.0). All rights for text and data mining, AI training, and similar technologies for commercial purposes, are reserved. ISSN 1824-8039. Published by SISSA Medialab.

<https://pos.sissa.it/>

1. Introduction

Accreting compact binaries provide a convenient laboratory for studying accretion disc properties and its variability. In compact binaries, mass transfer via Roche lobe overflow onto a compact object leads in most cases to the formation of an accretion disc, whose structure and variability carry information about the physical processes governing accretion. The central object can be a black hole (BH) or a neutron star (NS), as in X-ray binaries (XRBs; [6]), or a white dwarf (WD) in the case of accreting white dwarfs (AWDs; Solheim 42, Warner 50).

Most AWDs fall under the category of cataclysmic variables (CVs), which accrete from a main sequence-like donor. The magnetic field strength of the WD can strongly influence the dynamics of the accretion flow. For field strengths $\gtrsim 10^6$ G, the inner disc is truncated at the magnetospheric radius, and material is channelled along magnetic field lines onto the WD magnetic poles. Systems in which the spin of the WD is not synchronised with the binary orbit usually have the inner accretion disc truncated at the magnetospheric radius and are referred to as Intermediate Polars (IPs; Norton et al. 30, 31). In the case where the magnetic field is $\gtrsim 10^7$ G and the spin is synchronised with the orbit no accretion disc is formed as the magnetospheric radius is beyond the circularisation radius. Instead accretion proceeds exclusively along field lines and these systems are classified as Polars (Cropper 5). The interaction between the accretion flow and the magnetic field thus plays a central role in shaping the observable properties of AWDs.

Quasi-periodic oscillations (QPOs) are a common manifestation of non-coherent luminosity variability and have been extensively studied in XRBs [e.g. 19, 52]. They appear as broad, Lorentzian-like features in the power density spectrum (PSD), reflecting quasi-stable modulations in the emitted flux. The quality factor, defined as $Q = \nu_0 / (2\Delta)$, where ν_0 is the centroid frequency and Δ the half-width at half-maximum, quantifies their coherence. In XRBs, a subtype of QPOs, Type-C QPOs in black hole XRBs and type HBO QPOs in neutron star XRBs, are of particular interest, exhibiting strong harmonics and a well-defined correlation between ν_{QPO} and the broadband low-frequency break ν_b [52]. Such behaviour is widely interpreted as a signature of geometric precession of the inner accretion flow, driven by the Lense–Thirring effect in the presence of misalignment between the disc and the compact object spin axis [20].

While QPOs have been recognised as a ubiquitous feature in XRBs, their analogues in AWDs have long remained elusive. Early reports of transient, quasi-coherent oscillations and dwarf nova oscillations (DNOs) in systems such as WZ Sge [51] suggested that similar processes might operate in accreting WDs, though the transient nature of those signals and the lack of accompanying harmonics indicated a potentially distinct physical origin. The recent detection of persistent optical QPOs in AWDs by [48] has, however, provided the first evidence that self-similar accretion-driven variability exists across the accreting binary mass scale. [48] reported discovery of five AWD systems exhibiting persistent QPOs at frequencies $\sim 1.3\text{--}3 \times 10^{-4}$ Hz (periods of $\sim 1\text{--}2$ h) in the *Transient Exoplanet Satellite Survey (TESS)*. Similarly to the Type C QPOs in XRBs, three of these systems display harmonics—constituting the first such detection for QPOs in AWDs. The QPOs were identified using time-averaged power spectra (TPS) constructed following standard XRB timing procedures, and their properties (broad-band noise, QPO frequency, and low-frequency break) follow a correlation consistent with the [52] relation, establishing a direct observational link between AWDs and XRBs.

To interpret these results, [48] implemented a physical model in which the observed QPOs arise from magnetically driven precession (MDP) of the inner accretion flow, originally developed by [24]. In the framework of the MDP model the interaction between a weakly magnetised, tilted WD dipole and the inner disc induces warping and global precession of the disc. The resulting precession modulates the visibility and projected area of the hot inner flow, producing quasi-periodic brightness variations. The MDP mechanism naturally explains the persistence and moderate coherence of the observed QPOs, and the presence of harmonics through asymmetries introduced by disc warping or magnetically confined structures.

The same physical process has been invoked to explain mHz QPOs in pulsating ultraluminous X-ray sources (PULXs; [9, 22, 23, 36]), such as M82 X-2 and M51 ULX-7, where highly magnetised neutron stars accrete at super-Eddington rates [49]. In these systems, the observed QPO frequencies are consistent with magnetospheric precession at or near the truncation radius. This similarity underscores the importance of magnetospheric torques in shaping accretion-driven variability across compact object classes.

Overall a larger sample of AWDs showing XRB-like QPOs is needed to provide compelling evidence that magnetically driven precession operates in weakly magnetised AWDs. With 2 out of 5 AWDs showing these QPOs in [48] being WZ Sge type stars, including the WZ Sge itself a closer inspection of similar systems is needed. BW Scl is a close-by and bright WZ Sge type dwarf nova (Distance $\sim 93.6 \pm 0.5$ pc [4]). BW Scl is also thought to be at the beginning stages of its period bounce [29, 35] with a precise ephemeris derived from *TESS* and *AAVSO* data provided by [29]. BW Scl is also recorded to be a soft X-ray source by *ROSAT* [1] as RX J2353.0-3852. The binary parameters of the system were in detail explored by [29] through Doppler tomography, suggesting that BW Scl donor is a T spectral type brown dwarf with mass ($M_2 = 0.051 \pm 0.006 M_\odot$) below the hydrogen-burning limit. They also constrained the mass of the white dwarf to $M_{WD} = 0.85 \pm 0.04 M_\odot$ and derived an upper limit on the accretion rate from the optically thin quiescent accretion disc as $\lesssim 7 \times 10^{-13} M_\odot \text{yr}^{-1}$. These characteristics make BW Scl an ideal target for testing WZ Sge analogous QPOs.

In this work in Section 2 we provide a description of the data used in this work and in Section 3 we introduce the MDP model in detail as well as the fiducial parameters and their values. In Section 4.1 we report here the detection of a new QPO in the *TESS* data in the quiescent state of WZ Sge type DN BW Scl. In Section 4.2 we introduce the new method of parameter space exploration for the MDP model used in [49] here adapted for the AWD case. Section 5 contains the discussion of the results obtained in this work. In particular in Section 5.1 we discuss the application of the MDP model to the new QPO in BW Scl and explore the parameter space of the model, similarly to [49]. In Section 5.2 we discuss the implications of this new parameter space exploration compared to the results in [48] and in Section 4.1.

2. Data

All data reported here were obtained by *TESS* and is publicly available at the Mikulski Archive for Space Telescopes (MAST¹). *TESS* is a space-based near-all sky survey which has been in

¹<https://mast.stsci.edu/portal/Mashup/Clients/Mast/Portal.html>

operation since 2018 and has covered $\sim 95\%$ of the sky. It operates with a wide optical to near infrared filter (600 – 1000 nm). Thanks to its large field of view (FOV)($24^\circ \times 96^\circ$) it observes a large portion of the sky in so-called Sectors, which span approximately 27 days. For all targets in the FOV which are a part of a guest observer program *TESS* provides high cadence time series with time resolution of 20 s or 2 mins. Additionally for all covered FOV full frame images are made available at a lower cadence which has evolved during the extended missions from 30 mins to current 10 mins. With such vast coverage and excellent timing capabilities *TESS* provides the ideal setup for systematic studies of variability of accreting systems, particularly AWDs. Furthermore, it provides an indispensable testing ground for new and more single field focused missions such as *PLATO* [38], which will be able to provide the colour information on a subset of *TESS* targets.

The data discussed in Section 4.2 has been previously published in [48] and it is discussed there in detail. Here we only consider the QPO frequencies reported in [48]. Data used in Section 4.1 pertains to a WZ Sge type star BW Scl, which was observed by *TESS* on 2 occasions. First it was observed in Sector 29 from 26th of August 2020 to 21st of September 2020 and then in Sector 69 from 25th of August 2023 to 20th of September 2023. On both occasions 20 s cadence data was obtained.

The data was downloaded and treated for cosmic rays using the *Lightkurve* package² [25]. Due to bad background subtraction in the automatic light curve production an in-house pipeline was used to re-reduce the data using custom masks for the source and the background. Some data was also discarded as it was affected by a background flare and no usable scientific information could have been extracted. The reduced data for both *TESS* Sectors is shown 1 with a time averaged light curve on the timescale of the QPO shown in black as well.

3. Magnetically Driven Precession QPO model

In this Section we summarise the Magnetically Driven Precession (MDP) QPO model as implemented in [48]. In XRBs the preferred model for explaining QPOs, particularly in the BH case has been the Lense-Thirring precession [11, 20, 37, 43, 44]. Lense-Thirring precession induces the precession of a warped inner accretion flow due to a relativistic effect of frame-dragging. However, in NS XRBs it is also important to consider the accretor magnetic field as a potential contributor to accretion disc warp generation. There have been several models that proposed how the neutron star magnetic field can affect the geometry of the accretion disc and its behaviour. [2] suggested that at the radius where the NS magnetic field is comparable to that of the accretion disc the resulting interactions between the fields can result in a QPO-like behaviour. However considering the comparatively smaller magnetic field of WD accretion discs, this is not a viable option.

Another magnetic field driven option was proposed by [24]. There, a model for QPOs was proposed for NS XRBs and T Tauri stars where similarly to Lense-Thirring precession a wobbling motion of the inner accretion disc is the driving mechanism of the QPO. However in [24] the source of the precession is a magnetic torque on the accretion disc produced by an offset magnetic momentum and spin axis of the accretor to the angular momentum of the outer geometrically thin

²<https://github.com/lightkurve/lightkurve>

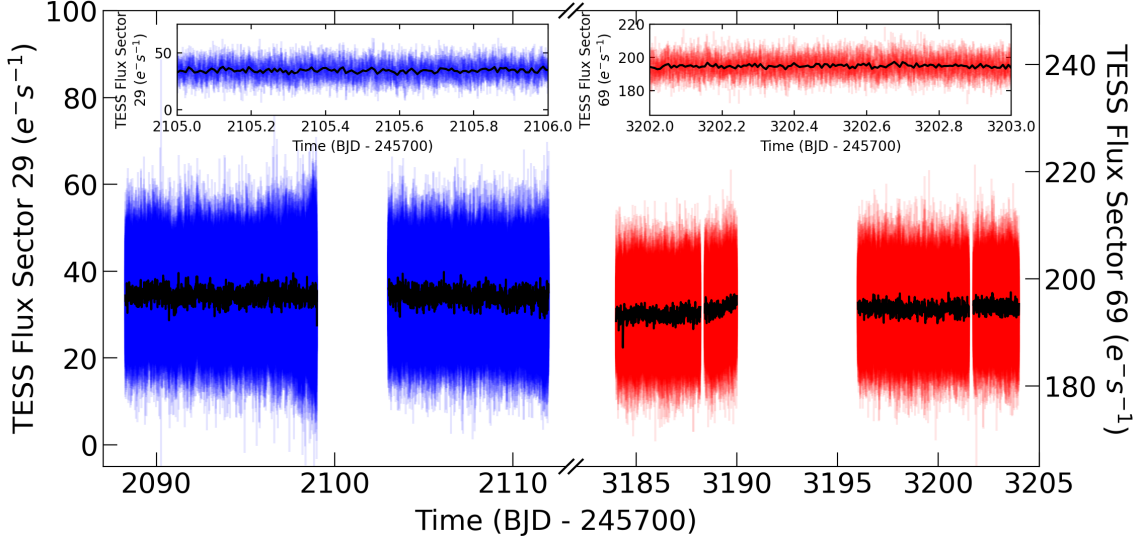


Figure 1: Light curve of BW Scl showing all sectors of *TESS* data as described in Section 2. The gap between the individual *TESS* Sectors has been excluded. The solid black line in each panel denotes the running average of the light curve on the QPO timescale. The upper inset plots show a 1-day zoom in of the light curves for each Sector to highlight the QPO variability.

and optically thick accretion disc. The torque then produces a warping effect on the inner accretion disc resulting in a wobbling motion of the warped part of the accretion disc. The light emitted by the warped region is the source of the quasi-periodic variation in the light curve, based on its orbit around the accretor. The characteristic orbit of the warped disc region is governed by the accretor dipole and hence will predominantly occur at the magnetospheric radius r_M of the system:

$$r_M = \eta \left(\frac{2\pi^2}{\mu_0^2} \frac{\mu^4}{GM\dot{M}^2} \right)^{\frac{1}{7}}, \quad (1)$$

where η is a dimensionless parameter describing the offset between the Alfvén and magnetospheric radius due to the geometrical differences induced by the ram pressure and the tilt of the magnetic field with respect to the plane of the accretion disc. In NS XRBs this parameter is usually set to 0.5 [15, 28]. However, in systems with low magnetic field this factor could have much lower values as suggested in [48] or similarly in systems with high inclination. μ_0 is the magnetic vacuum permeability and μ the stellar magnetic dipole moment such that $\mu = BR^3$, where the B is the magnetic field strength and R the accretor radius. G is the gravitational constant, M the accretor mass and \dot{M} the instantaneous accretion rate onto the accretor.

Therefore theoretically the main factors affecting the radius at which the QPO occurs in NS XRBs is governed by the accretor magnetic field and accretion rate. However, in general a simplifying assumption can be made that if the system is in spin equilibrium then the radius is also equal to the corotation radius r_{CO} , such that:

$$r_{\text{CO}} = \left(\frac{GMP_{\text{spin}}^2}{4\pi^2} \right)^{\frac{1}{3}}, \quad (2)$$

where P_{spin} is the spin period of the accretor. Hence assuming that the precession of the entire inner disc can be approximated by a precession of a single disc ring at $r = r_{\text{M}} = r_{\text{CO}}$ [24] presents an expression for the precession frequency $\nu_{\text{p}}(r)$ with an offset A between the global precession frequency and the magnetically driven precession frequency. The offset can be $A \simeq 0.3 - 0.85$ as determined by [41], depending on the detail of the inner disc structure. Therefore the QPO frequency can be expressed as:

$$\nu_{\text{QPO}} = A \frac{\Omega_{\text{p}}(r_{\text{in}})}{2\pi} = \frac{A}{2\pi} \frac{\mu^2}{\pi^2 r^7 \Omega(r) \Sigma(r) D(r)} F(\theta), \quad (3)$$

where Ω_{p} is the angular precession frequency associated with ν_{p} , $\Omega(r)$ is the Keplerian frequency associated with the QPO radius r , $\Sigma(r)$ is the corresponding surface density. The surface density term here is hence the main point at which the assumed accretion disc model affects the model predicted properties of the QPO, like its scaling with accretion rate and other observables. In [24] as well as [48] the accretion disc is assumed to be standard geometrically thin and optically thick disc as described by [40]. Hence the expression for surface density here is adopted as shown in Eq. 5.41 in [12]. $D(r)$ is a dimensionless function depending on the disc height (see details in [24] and Appendix C in [48]). Lastly $F(\theta)$ is also described in Appendix C of [48] and gives a measure of the type of magnetic field that is being screened out (vertical or spin variable).

4. Results

In Section 4.1 we report the identification of a non-coherent signal in *TESS* data of a WZ Sge type dwarf nova. In Section 4.2 we report the comprehensive analysis of the MDP parameter space of AWD QPOs reported in [48].

4.1 Detection of a new QPO in BW Scl

Here we discuss the non-coherent signal seen in *TESS* data of BW Scl reported in [29] and its empirical characterisation. In [29] the signal at $\sim 68\text{c/d}$ was reported as a 'quiescent superhump' with time-variable peaks and low amplitude, where c/d is analogous to d^{-1} . A similar photometric variability was also reported at these frequencies by [46]. Here we re-analyse this variability and interpret it as a QPO analogous to those seen in other AWDs [48] and explore its interpretation under the framework of the MDP model in the discussion in Section 5.1.

The *TESS* light curve of Sector 29 is reported in [29] and it is shown with Sector 69 in Figure 1. Here we follow the procedure of constructing a time-averaged power spectrum (TPS) as described in [48]. This method briefly consists of segmenting the light curve into sections of equal length and minimising the gaps in the data. The segments length used here is 5 days - this is chosen to maximise the number of segments as well as their length. Whereas in [48] some segments could be up to ~ 10 days, here with only one *TESS* Sector where the QPO is seen number of segments is prioritised over their length. With the chosen segment length a Lomb-Scargle periodogram [27]

is computed for each segment. In the frequency domain the peaks associated to the orbital period are removed for the first 3 harmonics. The harmonics are removed by masking 25 data points on each side of the peak of each harmonic. 3 harmonics are chosen as a conservative estimate as only 2 are identified by visual inspection. Then the segments are averaged together and re-binned on a frequency grid with 100 bins. Again this number is chosen arbitrarily within the range of number of bins for which the results are robust. The TPS for both sectors is shown in Figure 2 with an inset displaying the non-averaged PSD zoomed in on the orbital period and its harmonic.

In the non-averaged PSD of Sector 29 the orbital period and its first harmonic are recovered and are consistent with the ephemeris obtained in [29] with $P_{\text{orb}} = 18.4080994 \pm 8 \text{ c/d}$. A QPO is visible at 68 c/d also as observed by [29]. In the TPS of Sector 29 after the removal of orbital variability the QPO is clearly visible and is fitted with a single Lorentzian. The broad-band variability component is fitted with a single zero-centred Lorentzian and the Poisson noise is represented by a constant. The overall expression for the TPS fit is hence:

$$P_{\nu} = P_{\text{L}}(r_1, \Delta_1, \nu_0, \nu) + P_{\text{L}_0}(r_2, \Delta_2, \nu) + A, \quad (4)$$

where A represents the Poisson noise constant and P_{L} and P_{L_0} represent the QPO and broad-band zero-centred Lorentzian respectively such that:

$$P_{\text{L}}(\nu) = \frac{r^2 \Delta}{\pi} \frac{1}{\Delta^2 + (\nu - \nu_0)^2}, \quad (5)$$

where $P_{\text{L}}(\nu)$ is the RMS normalised power, Δ the half width half maximum (HWHM) and r a normalisation factor proportional to the integrated fractional rms. ν_0 represents the centroid frequency, which is set to 0 in the case of zero-centred Lorentzians. In the case of non-zero centred Lorentzians, where $\nu_0 > 0$, the frequency of the peak of the PSD feature is given by:

$$\nu_{\text{max}} = \sqrt{\nu_0^2 + \Delta^2}. \quad (6)$$

The Poisson noise level is lower in Sector 69, however with minimum close to no intrinsic broad-band variability at frequencies $\gtrsim 10^{-5} \text{ Hz}$. Hence the QPO Lorentzian is omitted from the fit. This is also visible from the non-averaged PSD inset in Figure 2 where no power excess is visible at the QPO frequencies from Sector 29. The individual values for the TPS fits are hence shown in Table 1.

4.2 Parameter space investigation of Magnetically Driven Precession model

In this Section we discuss the results from comprehensive parameter space exploration of the MDP model for QPOs in AWDs reported in [48] and for BW Scl reported in Section 4.1. [48] chose a set of fiducial parameters when applying the model to the AWD QPOs in order to explore the magnetic field and accretion rate dependence. This however required a substantial number of assumptions on the parameters, such as the accretion disc viscosity α . Since the nature and behaviour of α in standard Shakura-Sunyaev accretion discs is not yet well understood, here we stand to conduct a parameter exploration without such dependence. Furthermore [48] relied on the Disc Instability Model (DIM) deductions of α from the recurrence times of outbursts in WZ Sge and GW Lib. Due to the unusually low accretion rates in WZ Sge type stars ($\dot{M} \lesssim 10^{-11} M_{\odot} \text{ yr}^{-1}$),

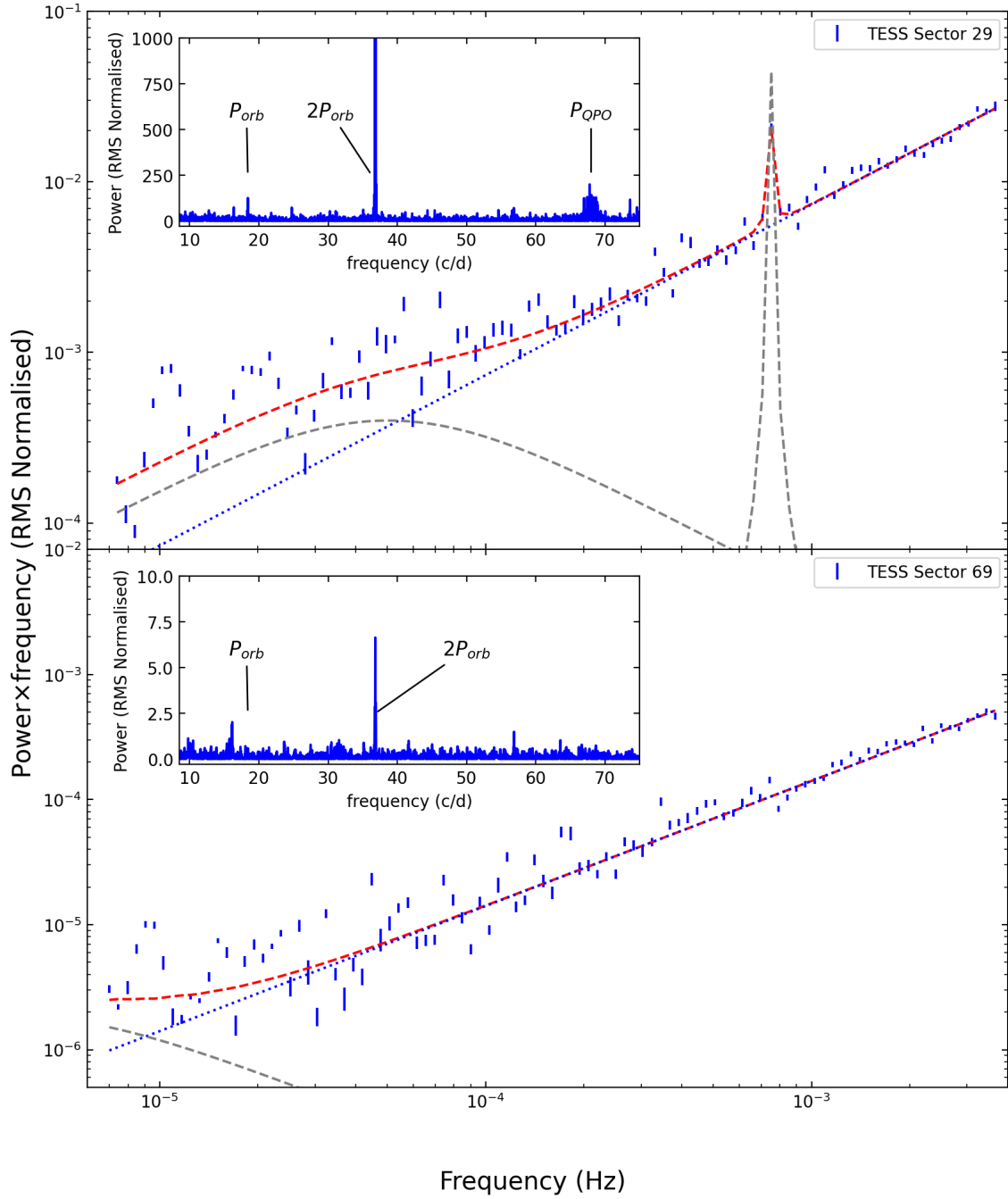


Figure 2: TPS of both Sectors of *TESS* data of BW Scl averaged on 5-day segment length with 100 logarithmically spaced bins. The empirical fit of the PSD is included here and comprises a Poisson noise power law (dotted line) in the high frequencies, one zero-centred Lorentzians (solid line) representing the broad band PSD structure and Lorentzians representing the QPOs and their harmonics (dashed line). The inset shows a section of the non-averaged PSD between $\sim 10 - 75$ c/d.

Table 1: Results of the empirical fit to the TPS from Figure 2. The independent rows correspond to different Sectors and the columns correspond to model components: A – Poisson noise amplitude, r_i – integrated fractional rms of a given Lorentzian, Δ_i – half width half maximum of a given Lorentzian, $\nu_{0,1}$ – centroid frequency of a given Lorentzian (only Lorentzians representing QPOs and their harmonics have this component). The Q value for the non-zero centred Lorentzian representing a QPO is given as well and is denoted by Q . Broad-band component Lorentzians are zero-centred and their $\nu_0 = 0$ by default and is not denoted here.

Sector	A	r_1	Δ_1	$\nu_{0,1}$	Q	r_2	Δ_2
Sector 29	7.4 ± 0.4	$3_{-2}^{+1} \times 10^{-2}$	$5 \pm 4 \times 10^{-2}$		~ 80	$5 \pm 4 \times 10^{-2}$	$5 \pm 1 \times 10^{-5}$
Sector 69	$0.141_{-0.003}^{+0.003}$	–	–	–	–	$3_{-3}^{+7} \times 10^{-3}$	$4_{-4}^{+3} \times 10^{-6}$

the inferred values of α may not be representative of the other higher accretion rate systems in the sample (i.e. T Pyx [16] and CP Pup [47]). Furthermore it is still a standing question as to the reason behind the long recurrence timescales of outbursts in WZ Sge type stars. One option is to indeed invoke very low values of viscosity. Another option is to have truncated inner disc, such as implied by the colour of CVs in the *Gaia* colour magnitude diagram (CMD) [7].

With this in mind we aim to conduct a comprehensive parameter search of the QPO parameter space as done in [49]. There the entire parameter space was randomly sampled for an application of the MDP model to new types of QPOs found in pulsating ultraluminous X-ray sources (PULXs), particularly M82 X-2 [3, 10, 26], M51 ULX-7 [8, 18, 39] and NGC 7793 P13 [13, 14, 21]. The parameter ranges considered for AWDs are summarised in Table 2 alongside the 2 last fiducial parameters, i.e. the WD mass and radius. These are fixed to their fiducial values due to the low expected scatter [33] and the consequent effect on the MDP QPO frequency prediction.

Therefore the model is evaluated 10^8 times, with the input parameters being randomly selected from uniform distributions of the parameter ranges from Table 2. All model evaluations for which the resulting QPO frequency is within the uncertainty of the measured value are recorded. The resulting corner plot of these combinations is shown in Figures 3 for WZ Sge and Figure 4 for GW Lib as grey circles. Figure 6 shows the corner plot for BW Scl and Figure 5 shows all three parameter spaces for CP Pup, T Pyx and V3101 Cyg, i.e. the other QPOs reported in [48]. As it is visible in the corner plots, this does not produce significant constraint on most of the model parameters as in the PULX case in [49]. Hence further constraints are inferred from independent accretion rate and spin measurements. This is done by evaluating the model further 10^8 times, but restricting the sampling of the accretion rate to the observed ranges shown in Table 3. The corresponding model evaluations reproducing the QPO frequency are denoted by red diamonds in the aforementioned corner plots. An analogous constraint is then added on the spin period, when available, i.e. WZ Sge [34] and GW Lib [45]. Blue squares hence denote the model parameter combinations where all three constraints on QPO frequency, accretion rate and spin are met.

Whereas even these conditions cannot produce further constraints on some model parameters (disc viscosity α and disc offset θ) the recovered distributions of the magnetic field B and offset of η show a normal distribution. The distribution parameters are reported in Table 4. It is imperative here to note that these distributions do not represent the likelihood of the parameter values, merely the number of potential solution combinations that returned the appropriate QPO frequency, accretion

Table 2: Model parameters for the magnetically driven precession model for QPOs in AWDs. Parameters with their explored ranges are given. For some cases they are fixed to a fiducial value, where only that one is given and denoted by *.

Model Parameter	Value
M^* (M_{\odot})	0.8
R^* (R_{\odot})	0.01
B (G)	$10^3 - 10^{11}$
\dot{M} ($M_{\odot}yr^{-1}$)	$10^{-15} - 10^{-4}$
α	$10^{-6} - 1$
η	$10^{-5} - 1$
θ ($^{\circ}$)	0 - 90
A^*	0.65

Table 3: Accretion rates assumed here for AWD systems showing type-C analogous QPOs along with the corresponding publications. The only systems where a single value is quoted without an error are GW Lib and BW Scl, for which purposes a 10% error margin is assumed.

System	\dot{M} ($M_{\odot}yr^{-1}$)	Reference
WZ Sge	$7.4 \pm 1.3 \times 10^{-11}$	[32]
GW Lib	7×10^{-14}	[17]
CP Pup	$1 - 2 \times 10^{-10}$	[47]
T Pyx	$10^{-7} - 10^{-6}$	[16]
V3101 Cyg	$10^{-11} - 10^{-10}$	[48]
BW Scl	$\lesssim 7 \times 10^{-13}$	[29]

Table 4: Limits and ranges for MDP model parameters for QPOs in AWDs. B lower limit is derived using the \dot{M} constraint, whereas $\log(B)$ range uses the spin limitation as well, where available. $\log(\eta)$ is the range as obtained from the entire parameter space, and the \dot{M} constraint is marked by * and adding spin constraint as well is denoted by †.

Model Parameter	CP Pup	WZ Sge	GW Lib	T Pyx	V3101 Cyg	BW Scl
B (G)	$> 3 \times 10^3$	$> 7 \times 10^2$	$> 1 \times 10^3$	$> 8 \times 10^4$	$> 9 \times 10^2$	$> 3 \times 10^2$
$\log(B)$ ($\log(G)$)	–	5.4 ± 0.8	5.8 ± 0.8	–	–	–
$\log(\eta)$	-1.5 ± 0.6	-1.5 ± 0.6	-1.4 ± 0.6	-1.5 ± 0.6	-1.5 ± 0.6	-1.6 ± 0.6
$\log(\eta)^*$	-1.4 ± 0.5	-1.6 ± 0.5	-1.6 ± 0.5	-1.1 ± 0.5	-1.5 ± 0.5	-1.8 ± 0.5
$\log(\eta)^{\dagger}$	–	-1.2 ± 0.5	-1.4 ± 0.5	–	–	–

rate and WD spin. Hence all values within the distribution range should be treated as having equal likelihood of representing the system parameters.

5. Discussion

In this Section we first discuss the physical interpretation of the QPO in BW Scl under the framework of the MDP model in Section 5.1. Then, in Section 5.2 we discuss the implications of

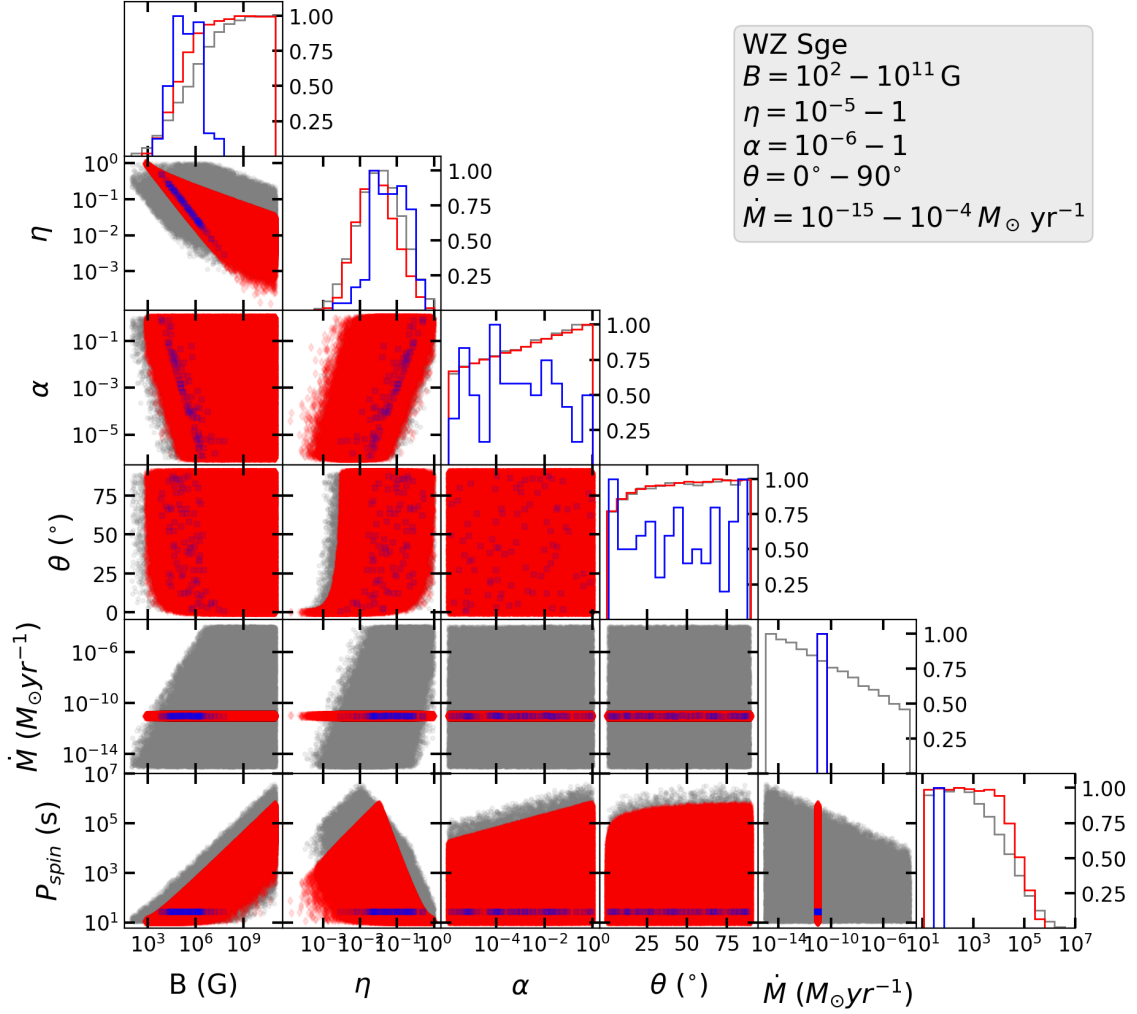


Figure 3: Parameter space of the MDP model with all parameter combinations (in grey circles) producing QPO frequency and spin within the observed errors as noted in [48] and 3. All the solutions which also reproduce accretion rate within the range given in Table 3 are given in red diamonds. The blue squares represent fractions of family of solutions of the red diamonds, that also reproduce the spin of WZ Sge within its error as given in [34]. Distributions of all parameters are provided, with all being scaled to unity. The explored parameter ranges are noted as also shown in Table 2.

the reanalysis of the MDP parameter space of QPOs from [48].

5.1 Nature of QPO in BW Scl

Considering the observational similarities of the QPO in BW Scl reported in Section 4.1 we now consider the interpretation of the physical mechanism driving the phenomenon. Similarly to [48] we apply the MDP model to explain the QPO behaviour. We adapt the same technique of evaluating the QPO parameter space as described in Section 4.2. However as opposed to the systems discussed there, we adapt a white dwarf mass of $M = 0.85 \pm 0.04 M_{\odot}$ and the associated white dwarf radius $R = 0.0094 \pm 0.0004 R_{\odot}$ from [29]. All other parameters and their ranges in

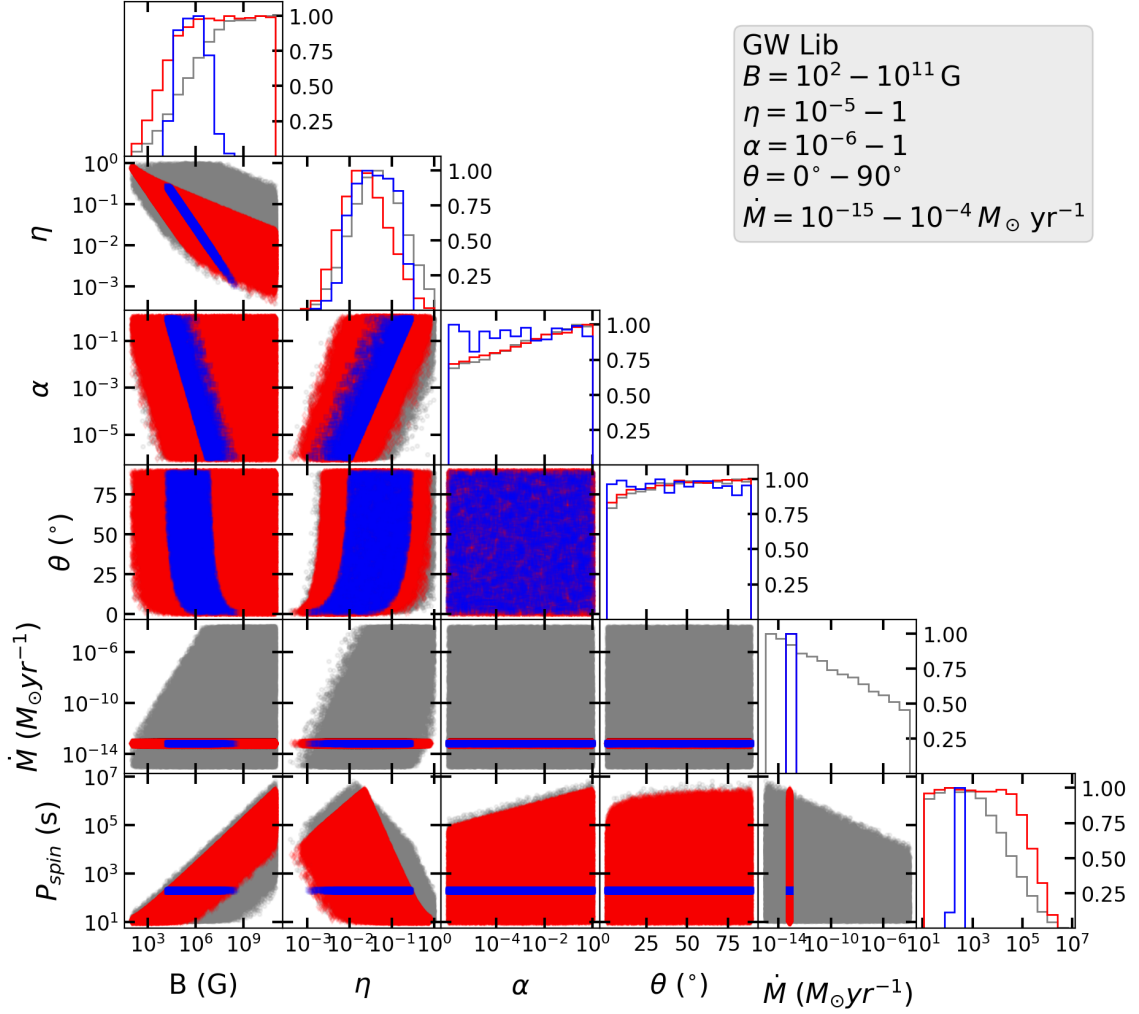


Figure 4: Parameter space of the MDP model with all parameter combinations (in grey circles) producing QPO frequency and spin within the observed errors as noted in [48] and 3. All the solutions which also reproduce accretion rate within the range given in Table 3 are given in red diamonds. The blue squares represent fractions of family of solutions of the red diamonds, that also reproduce the spin of GW Lib as given in [45]. Distributions of all parameters are provided, with all being scaled to unity. The explored parameter ranges are noted as also shown in Table 2.

Table 4 are kept the same. The resulting parameter exploration leads to the possible solutions as shown in Figure 6. The accretion rate constraint is taken from [29] as $\dot{M} \sim 7 \times 10^{-13} M_{\odot} \text{yr}^{-1}$.

5.2 Implications of broader parameter space exploration in the MDP model of QPOs in AWDs

Considering the wider exploration of the parameter space of the MDP model in the AWD application it is necessary to re-evaluate the conclusions of [48] and discuss new implications. Similarly to the PULXs[49], the overall distributions of individual parameter values across all families of solutions for the QPO can provide limits on specific parameters. These limits, mostly

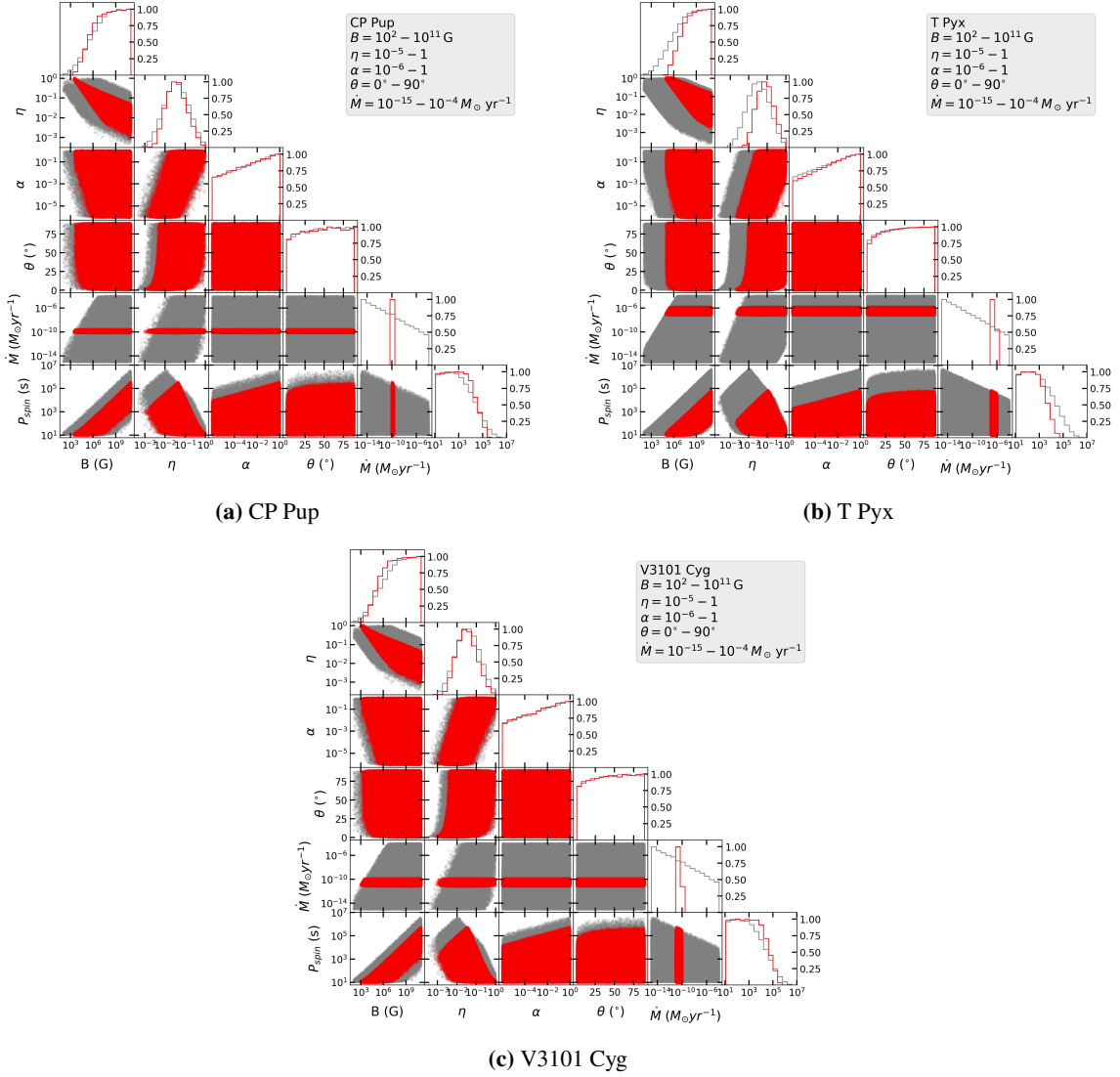


Figure 5: Parameter space of the MDP model for three accreting white dwarf systems. Grey circles show all parameter combinations producing QPO frequency consistent with observations, while red diamonds indicate solutions that additionally reproduce the observed accretion rates listed in Table 3. All parameter distributions are scaled to unity, and the explored parameter ranges are given in Table 2.

drawn from the \dot{M} constraint family of solutions relies therefore not only on the model assumptions but also on the \dot{M} measurement. However, using this limit it is possible to extract lower limits on the B for all systems, and even constrain a range of possible values. The range, given by the mean and standard deviation of the distribution in Figures 3 and 4 is constrained using the spin period. The respective values of the limits and ranges are summarised in Table 4. Similar estimates can also be provided for the η parameter and are also summarised in Table 4.

Fixing specific parameters in the MDP model to fiducial values like in [48] allowed for rough estimates on the spin periods of the systems without a pre-existing measurement. However, when considering a larger parameter space for the MDP model as in this section, this is not possible, bar

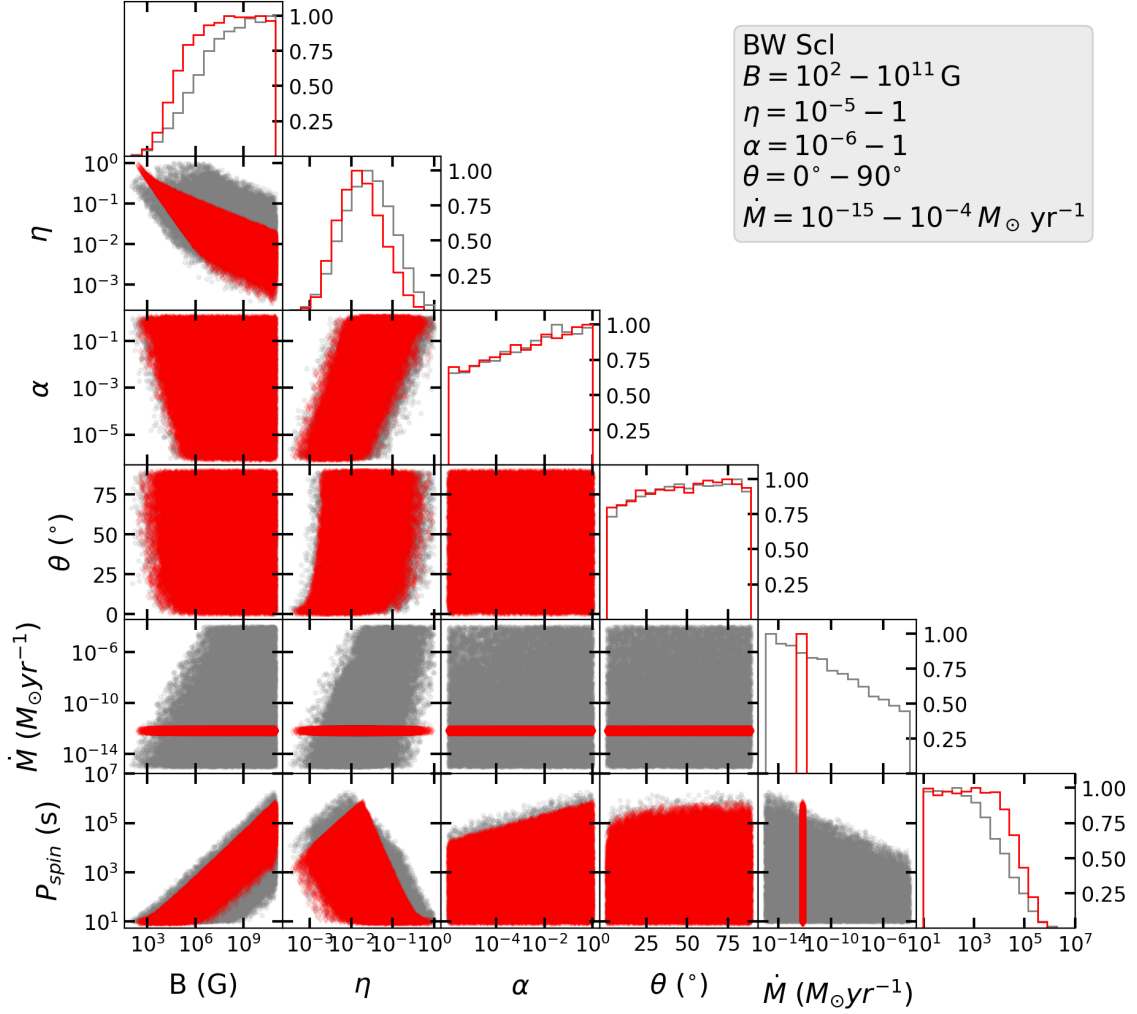


Figure 6: Parameter space of the MDP model with all parameter combinations (in grey circles) producing QPO frequency and spin within the observed errors as noted in Table (reference). All the solutions which also reproduce accretion rate from [29] are given in red diamonds. Distributions of all parameters are provided, with all being scaled to unity. The explored parameter ranges are noted as also shown in Table 2.

a very rough upper limit. Overall, without a separate handle on some of the other parameters, such as α or B , the spin estimates for these systems may remain elusive.

6. Conclusions

In conclusion, we report the detection of a QPO in the WZ Sge-type dwarf nova BW Scl, making it the sixth nearby system of this class to exhibit XRB-like QPO behaviour and sixth overall AWD QPO. Through a reanalysis of previously reported AWD QPOs and the application of a comprehensive parameter space exploration of the MDP model, we demonstrate that such QPOs can be consistently interpreted as arising from magnetically induced precession of the inner accretion flow. Importantly, this approach avoids reliance on fiducial parameter assumptions and

highlights the intrinsic degeneracies of the model when applied across a broad parameter space.

Despite these degeneracies, independent constraints on accretion rate and spin allow limits to be placed on key physical parameters, most notably the white dwarf magnetic field strength and the disc–magnetosphere coupling parameter. These results reinforce the view that QPOs in weakly magnetised AWDs represent a low-field analogue of similar phenomena observed in X-ray binaries and PULXs. AWDs therefore provide a valuable testbed for studying magnetically driven variability across compact object classes, and future high-cadence, long-baseline photometric monitoring such as *PLATO* will be crucial for expanding the sample and further constraining the underlying physical mechanisms.

References

- [1] Abbott T. M. C., Fleming T. A., Pasquini L., 1997, *A&A*, **318**, 134
- [2] Aly J. J., Kuijpers J., 1990, *A&A*, **227**, 473
- [3] Bachetti M., et al., 2022, *ApJ*, **937**, 125
- [4] Bailer-Jones C. A. L., Rybizki J., Foesneau M., Demleitner M., Andrae R., 2021, *AJ*, **161**, 147
- [5] Cropper M., 1990, *Space Sci. Rev.*, **54**, 195
- [6] Done C., Gierliński M., Kubota A., 2007, *A&A Rev.*, **15**, 1
- [7] Dubus G., Babusiaux C., 2024, *A&A*, **683**, A247
- [8] Earnshaw H. M., et al., 2016, *MNRAS*, **456**, 3840
- [9] Fabrika S. N., Atapin K. E., Vinokurov A. S., Sholukhova O. N., 2021, *Astrophysical Bulletin*, **76**, 6
- [10] Feng H., Rao F., Kaaret P., 2010, *ApJ*, **710**, L137
- [11] Fragile P. C., Mathews G. J., Wilson J. R., 2001, *ApJ*, **553**, 955
- [12] Frank J., King A., Raine D., 2002, *Accretion Power in Astrophysics*. 3rd edition, Cambridge University Press, doi:10.1017/cbo9781139164245.004
- [13] Fürst F., et al., 2016, *ApJ*, **831**, L14
- [14] Fürst F., et al., 2021, *A&A*, **651**, A75
- [15] Ghosh P., Lamb F. K., 1979, *ApJ*, **232**, 259
- [16] Godon P., Sion E. M., Williams R. E., Starrfield S., 2018, *ApJ*, **862**, 89
- [17] Hilton E. J., Szkody P., Mukadam A., Mukai K., Hellier C., van Zyl L., Homer L., 2007, *AJ*, **134**, 1503

- [18] Imbrogno M., et al., 2024, *A&A*, 689, A284
- [19] Ingram A. R., Motta S. E., 2019, *New A Rev.*, 85, 101524
- [20] Ingram A., Done C., Fragile P. C., 2009, *MNRAS*, 397, L101
- [21] Israel G. L., et al., 2017, *MNRAS*, 466, L48
- [22] Kaaret P., Feng H., Roberts T. P., 2017, *ARA&A*, 55, 303
- [23] King A., Lasota J.-P., Middleton M., 2023, *New A Rev.*, 96, 101672
- [24] Lai D., 1999, *ApJ*, 524, 1030
- [25] Lightkurve Collaboration et al., 2018, Lightkurve: Kepler and TESS time series analysis in Python, Astrophysics Source Code Library (ascl:1812.013)
- [26] Liu J., 2024, *ApJ*, 961, 196
- [27] Lomb N. R., 1976, *Ap&SS*, 39, 447
- [28] Mönkkönen J., Tsygankov S. S., Mushtukov A. A., Doroshenko V., Suleimanov V. F., Poutanen J., 2022, *MNRAS*, 515, 571
- [29] Neustroev V. V., Mäntynen I., 2023, *MNRAS*, 523, 6114
- [30] Norton A. J., Wynn G. A., Somerscales R. V., 2004, *ApJ*, 614, 349
- [31] Norton A. J., Butters O. W., Parker T. L., Wynn G. A., 2008, *ApJ*, 672, 524
- [32] Pala A. F., et al., 2020, *MNRAS*, 494, 3799
- [33] Pala A. F., et al., 2022, *MNRAS*, 510, 6110
- [34] Patterson J., 1980, *ApJ*, 241, 235
- [35] Patterson J., 2011, *MNRAS*, 411, 2695
- [36] Pinto C., Walton D. J., 2023, *arXiv e-prints*, p. arXiv:2302.00006
- [37] Psaltis D., Norman C., 2000, *arXiv e-prints*, pp astro-ph/0001391
- [38] Rauer H., Heras A. M., 2018, Space Missions for Exoplanet Science: PLATO, doi:10.1007/978-3-319-55333-7_86
- [39] Rodríguez Castillo G. A., et al., 2020, *ApJ*, 895, 60
- [40] Shakura N. I., Sunyaev R. A., 1973, *A&A*, 55, 155
- [41] Shirakawa A., Lai D., 2002, *ApJ*, 565, 1134
- [42] Solheim J.-E. S. E., 2010, *PASP*, 122, 1133

- [43] Stella L., Vietri M., 1998, *ApJ*, 492, L59
- [44] Stella L., Vietri M., Morsink S. M., 1999, *ApJ*, 524, L63
- [45] Szkody P., et al., 2012, *ApJ*, 753, 158
- [46] Uthas H., et al., 2012, *MNRAS*, 420, 379
- [47] Veresvarska M., Scaringi S., Hagen S., De Martino D., Done C., Ilkiewicz K., Knigge C., Littlefield C., 2024a, *MNRAS*, 529, 664
- [48] Veresvarska M., et al., 2024b, *MNRAS*, 534, 3087
- [49] Veresvarska M., et al., 2025, *MNRAS*,
- [50] Warner B., 2003, *Cataclysmic Variable Stars*, doi:10.1017/CBO9780511586491
- [51] Warner B., Woudt P. A., Pretorius M. L., 2003, *MNRAS*, 344, 1193
- [52] Wijnands R., van der Klis M., 1999, *ApJ*, 514, 939